


Melting upon Coalescence of Solid Nanoparticles

Reza Darvishi Kamachali 

Federal Institute for Materials Research and Testing (BAM), Unter den Eichen 87, 12205 Berlin, Germany; reza.kamachali@bam.de or reza.kamachali@gmail.com

Abstract: The large surface-to-volume ratio of nanoparticles is understood to be the source of many interesting phenomena. The melting temperature of nanoparticles is shown to dramatically reduce compared to bulk material. Yet, at temperatures below this reduced melting point, a liquid-like atomic arrangement on the surface of nanoparticles is still anticipated to influence its properties. To understand such surface effects, here, we study the coalescence of Au nanoparticles of various sizes using molecular dynamics simulations. Analysis of the potential energy and Lindemann index distribution across the nanoparticles reveals that high-energy, high-mobility surface atoms can enable the coalescence of nanoparticles at temperatures much lower than their corresponding melting point. The smaller the nanoparticles, the larger the difference between their melting and coalescence temperatures. For small enough particles and/or elevated enough temperatures, we found that the coalescence leads to a melting transition of the two nominally solid nanoparticles, here discussed in relation to the heat released due to the surface reduction upon the coalescence and the size dependence of latent heat. Such discontinuous melting transitions can lead to abrupt changes in the properties of nanoparticles, important for their applications at intermediate temperatures.

Keywords: molecular dynamics simulation; nanoparticles; phase transition; size effect



Citation: Darvishi Kamachali, R. Melting upon Coalescence of Solid Nanoparticles. *Solids* **2022**, *3*, 361–373. <https://doi.org/10.3390/solids3020025>

Academic Editors: Chee Kwan Gan and Guido Kickenbick

Received: 31 March 2022

Accepted: 1 June 2022

Published: 5 June 2022

Publisher's Note: MDPI stays neutral with regard to jurisdictional claims in published maps and institutional affiliations.



Copyright: © 2022 by the author. Licensee MDPI, Basel, Switzerland. This article is an open access article distributed under the terms and conditions of the Creative Commons Attribution (CC BY) license (<https://creativecommons.org/licenses/by/4.0/>).

1. Introduction

Due to their unique electronic, optical, and catalytic properties and relatively easy production [1–3], metallic nanoparticles have been at the forefront of nanotechnological advances [4–6]. In terms of application, the interactions between nanoparticles and their surrounding objects, such as solvents, substrates, ion/electron beams, as well as other nanoparticles, are of fundamental importance for optimizing their storage and performance [7–10]. The strong attraction among nanoparticles often results in their agglomeration, changing their desired functional properties. For instance, metallic/superconductor conjunctions [11], light scattering and absorption [12], and sorting [13] of nanoparticles are examples dealing with this challenge. Hence, studying nanoparticles' interactions is crucial to control and improve their synthesis, assembly, and application.

The surface energy of a nanoparticle can be a significant portion of its total energy, inversely increasing with its size. As a result, the surface has dramatic effects on the thermal stability of nanoparticles. It is well-known that the melting temperature of nanoparticles is also size-dependent, significantly lower than that of the bulk [14]. These make the interaction process strongly size-dependent, driven by a reduction in the total energy, mainly the surface energy, while having temperature-dependent kinetics. The interaction can involve either preserving the shape of the nanoparticles at low enough temperatures or changing their ultimate shape and size via a coalescence at higher temperatures. The latter can result in permanent agglomeration of the nanoparticles, with critical implications for their properties and performance. In this study, we explore the role of the surface reduction and its size dependence during the coalescence of gold (Au) nanoparticles and using the molecular dynamics (MD) simulation method.

Au nanoparticles are among the most interesting metallic nanoparticles that have found important applications in various contexts [15], e.g., as a remarkable catalyst [16–18], in printed

electronics [19], or in biotechnology [20]. The notable development of the Au nanoparticle is indebted to the noble nature of the element, remaining free of environmental contamination. In the shadow of its nobility, the interesting electronic properties and morphological diversity of Au nanoparticles were explored [21–23]. For high-temperature applications, both the phase and geometrical stability of Au nanoparticles become extremely important, often limiting their applications [24], but on certain occasions enabling their processing [25]. In either case, the temperature effects on nanoparticles need to be understood and controlled. The thermal sensitivity of Au nanoparticles is primarily dependent on their size but is also influenced by the shape of nanoparticles [26]. In a process of coalescence, both the size and shape of the nanoparticles vary, dynamically changing the thermal response of the nanoparticles. Such temperature-dependent features are most extreme in the coalescence of ultrafine particles.

In this work, we study the temperature and size dependence of the Au nanoparticles' coalescence. First, we consider the equilibrium melting behavior of single Au nanoparticles, to reveal their size-dependent thermal stability. We then study the coalescence of free nanoparticles. Detailed analyses of Lindemann index and potential energy distribution across the nanoparticles were performed to understand the mechanisms of nanoparticles' melting and coalescence. We reveal that the size-dependent surface effects can expand deep inside the nanoparticles, assisting with the coalescence at temperatures much lower than their melting temperature. For certain conditions discussed below, the surface energy released upon the coalescence adds to this effect, leading to the melting of the nominally solid nanoparticles during the coalescence.

2. Materials and Methods

For the current MD simulations, the glue potential for Au, created by the force matching method, is used [27]. The force matching method is an effective tool to obtain realistic interatomic potentials based on fitting the potential to ab-initio atomic forces of many atomic configurations [28,29]. The glue potential,

$$V = \frac{1}{2} \sum_{ij} \varphi(r_{ij}) + \sum_i U \left(\sum_j \rho(r_{ij}) \right) \quad (1)$$

contains a standard pair potential term $\varphi(r_{ij})$ and a so-called glue function $U(n_i)$, which is an energy associated with the coordination number of the atoms, $n_i = \sum_j \rho(r_{ij})$, with $\rho(r_{ij})$ being a short-range monotonically decreasing density function and r_{ij} representing the distance between i and j atoms. The glue potential has been successfully employed in several previous works for studying nanoparticles [30–32] and has also been shown to give reliable information on the surface properties of nanoparticles [33].

To perform the current simulations, modular software has been developed in MATLAB. We employed a listing algorithm for effectively updating the group of neighboring atoms. The Verlet velocity algorithm was used to solve the equations of motion. The desired temperature was obtained using the uniform kinetic energy scaling method, i.e., canonical sampling through velocity rescaling (CSVR). CSVR has been broadly used in MD simulations with applications to various problems [34,35]. This method best applies to studying heterogeneous melting phenomena and, particularly, for obtaining the equilibrium melting temperature and latent heat as we apply in the current study. The temporal constancy of temperature and energy with finite fluctuations has been carefully benchmarked. A small time-step of 1.7 fs guaranteed the convergence of the calculations. We considered fine Au nanoparticles with 586, 1289, and 2406 atoms. All nanoparticles were initially constructed to a perfect truncated polyhedral structure, as shown in Figure 1, that is the equilibrium Wulff structure for the FCC Au [36].

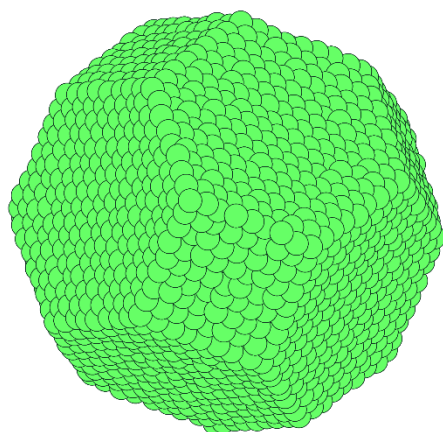


Figure 1. Initial nanoparticle structure. The nanoparticles were initially truncated polyhedrons with small random fluctuation in the atomic positions.

First, the melting points of the nanoparticles were approximated by studying the equilibrium potential energy as a function of temperature. A bulk system (NVT ensemble), i.e., a cubic simulation box of ten unit-cells per edge with a periodic boundary condition, has been simulated over a range of temperatures of interest for the purpose of (i) benchmarking our simulation tools, in particular the performance of the glue potential [27], and (ii) comparing the results against the nanoparticle systems to reveal the size-effect on the equilibrium melting temperature and latent heat. We also monitored the Lindemann index (LI) as a function of temperature, which gives extended insights about the activity of atoms within the system. The nanoparticles were equilibrated during an initial (minimum) 250,000 time-steps for each temperature, followed by another (minimum) 150,000 time-steps, depending on the system size, to average the values of potential energy and LI. For larger systems the equilibration needed more than 1,000,000 time-steps. The LI of each atom, δ_i , and of the entire nanoparticle, δ , was calculated by [37]

$$\delta_i = \frac{2}{N-1} \sum_{j \neq i}^N \frac{\sqrt{\langle r_{ij}^2 \rangle_T - \langle r_{ij} \rangle_T^2}}{\langle r_{ij} \rangle_T} \quad (2)$$

and

$$\delta = \frac{1}{N} \sum_i^N \delta_i, \quad (3)$$

respectively, where N is the number of atoms and $\langle \dots \rangle_T$ is the time average value at temperature T . The LI has been widely used for analyzing solid-liquid transitions but also provides excellent spatial information about the mobility and order of individual atoms across a given system. As a function of temperature, a sharp increase in the LI over a small temperature change reveals the melting point of the system [38,39]. Within the nanoparticles, the LI of individual atoms reflects on the atomic neighborhood and, in this case, surface-induced radial heterogeneities across the nanoparticle. In particular, the relative energy and mobility of surface atoms are interesting, to understand the physics of coalescence.

For studying the coalescence of nanoparticles, identical equilibrated Au nanoparticles of different sizes were brought into contact (separated by 0.2 nm) at different temperatures below and above their corresponding melting temperature. Each simulation has been studied for a minimum 200,000 time-steps. No external forces were applied during the coalescence. We note that the melting and coalescence of nanoparticles are heterogeneous (rather than homogeneous), which is due to the natural and significant role of free surfaces and edges. During the coalescence of nanoparticles, no temperature scaling is performed. Upon the coalescence, the mean diameter of the nanoparticles pair decreases. For a diameter

less than 10% of the minimum diameter, the coalescence is assumed to be completed [40]. The temporal evolution of the size, shape, energy, and temperature of the nanoparticles sheds light on the possible phase transition (melting) upon coalescence, which is discussed in the following. For more details on the simulation methods, see [41].

3. Results

Melting is a first-order phase transition involving a latent heat, i.e., an abrupt increase in the energy of the system. Figure 2a shows the potential energy for Au nanoparticles and the bulk system, computed as functions of temperature. Here, we study the equilibrium potential energy, as the temperature in all systems is kinetically scaled to the desired temperature [34,35], i.e., the nucleation of the liquid phase and its corresponding energy barrier do not appear as a part of the potential energy. In such a scaling process, superheating and associated metastable phenomena become irrelevant [42].

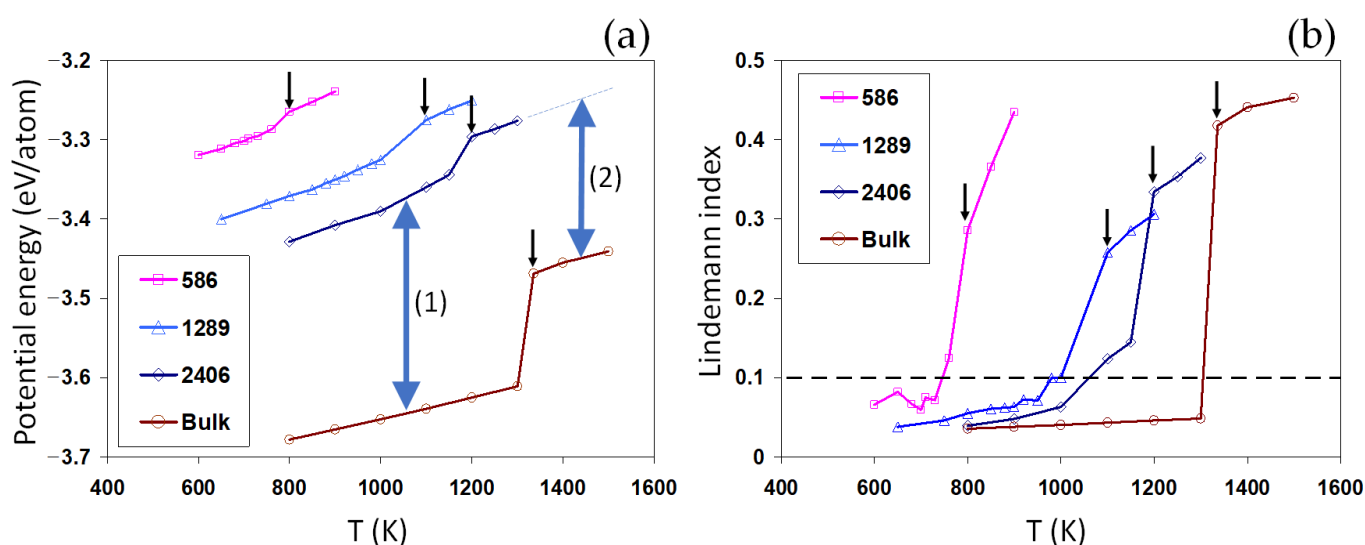


Figure 2. Melting of single nanoparticles. The potential energy (a) and the LI (b) of Au nanoparticles of different size and the reference bulk system are shown over temperature. Small arrows indicate the approximated melting point for each system. The two-sided arrow (1) and (2) indicates the increase in the overall potential energy for the solid and liquid nanoparticle, respectively.

For each curve in Figure 2a, the jump in the potential energy reveals the solid-liquid phase transition. The approximated melting temperatures are listed in Table 1. A good agreement is obtained here between the current results and previous works [43,44]. We note that the well-reproduced bulk melting temperature not only indicates the correctness of the current implementation of the glue potential [27], but also gives a reliable reference for comprehending the size-dependent melting properties of individual nanoparticles.

Table 1. Melting temperature (T_m), coalescence temperature (T_c), potential energy (E_p) and latent heat (L_m) of nanoparticles. * These values are approximations from computed simulation data points in Figure 2. ** The nanoparticle 586 is liquid at 800 K. 1 eV/atom = 96.45 kJ/mol.

No. of Atoms	Diameters (nm)	T_m (K) *	T_c (K)	$\frac{T_m - T_c}{T_m}$	E_p (eV/atom) at 800 K	L_m (eV/atom) *
586	~2.8	~800	~600	0.25	3.26 **	~0.013
1289	~3.6	~1100	~900	0.18	3.37	~0.028
2406	~4.5	~1200	~1000	0.16	3.43	~0.033
bulk	-	1336	-	-	3.67	~0.109

We found that the smaller the nanoparticle, the lower the melting point, which reflects the well-known Gibbs–Thompson size effect. Furthermore, the latent heat of melting is also found to be size-dependent, decreasing for smaller nanoparticles, as shown in Table 1. This confirms the size-dependent latent heat observed in the previous works [45,46].

At a given temperature, the potential energy of nanoparticles is significantly higher than the bulk values, increasing for smaller nanoparticles, indicated by the two-sided arrow (1) in Figure 2a. In the context of classical thermodynamics, this can be understood as the Laplace pressure induced by the surface energy (γ), equal to $2\gamma/R$, for a spherical particle of radius R . For the liquid nanoparticle, we found that the increase in the potential energy is much lower than the solid nanoparticle (two-sided arrow (2) compared to arrow (1), Figure 2a). This can be understood as the origin of the size-dependent latent heat for nanosystems. Interestingly, the size-dependent vertical shifts in the potential energy (indicated by the two-sided arrows) are found to be much larger than the melting latent heat of the nanoparticles and almost comparable to the latent heat for the melting in the bulk system. A small latent heat means a rather low energy barrier for melting. As the size of particles increases, the potential energy decreases and the latent heat increases, approaching the bulk values.

The spatial distribution of the potential energy across the nanoparticles can shed more light on the size-dependent energetics of the nanoparticles. Figure 3a–c compare the potential energy distributions of different nanoparticles. For each case, the distributions are shown at two temperatures corresponding to a solid and a liquid state, respectively. The horizontal lines present the average potential energy of the nanoparticles and the bulk system for the same temperatures. We have found that although the absolute energy difference between the two solid and liquid states can be relatively small, in the range of 0.1 eV/atom, the radial distribution greatly varies from the center to the surface. Core-shell heterogeneous energy distribution is evidenced within all nanoparticles, with a core region showing an almost uniform energy distribution rapped in a shell of high energy atoms. It is clear that a large number of atoms in the surface region of the nominally solid nanoparticle (for example Au₁₂₈₉ at 750 K, Figure 3b) have a much higher potential energy, even higher than the average potential energy of a liquid nanoparticle. This implies that it is possible for a premature surface melting to occur before reaching the melting temperature of the nanoparticle.

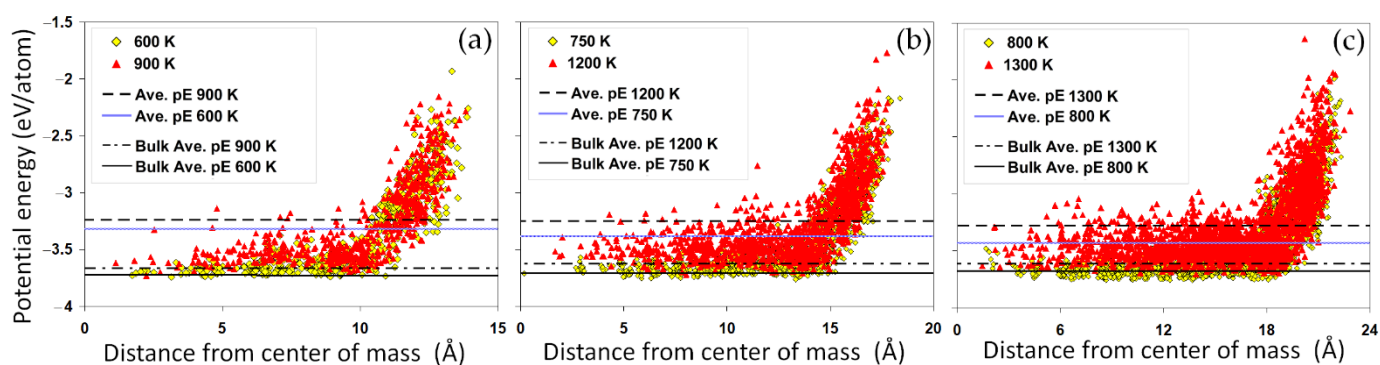


Figure 3. The radial distribution of the potential energy. The potential energy distributions for nanoparticles with (a) 586, (b) 1289 and (c) 2406 atoms are shown for two temperatures below and above their corresponding melting points. For comparison, the average potential energy of the nanoparticles and the bulk system are also shown (horizontal lines).

Similar to the potential energy, the average LIs, as shown in Figure 2b, indicate an abrupt increase upon the solid-liquid phase transition. The LI reflects on the average atomic mobility within each system. Thus, a sharp increase in this value, generally greater than 0.1, marks a solid-liquid phase transition. For the nanoparticles, while the sharpest increase in the LI values closely correlates with the jump in the potential energy, a significant

temperature-dependent increase is also visible below their corresponding melting point, indicating the possibility of a surface-induced premelting. To elaborate on the large LI values in the nanoparticles, we studied the radial distribution of atomic LI values across the nanoparticles, as shown in Figure 4a–c. The results show that a large portion of atoms in the nominally solid nanoparticles have a liquid-like high atomic LI value above 0.1. These results are consistent with the potential energy distribution shown in Figure 3a–c. This suggests that the surface plays a destabilizing role in the nanoparticles, thus increasing the mobility of surface atoms and therefore the LI values. Close to the melting point, the mobility of atoms and the corresponding LIs rapidly increase, enhancing the possibility of a surface melting phenomenon. For smaller nanoparticles, surface melting can occur over a wider range of temperatures, as shown in Figure 2b, with important implications for the coalescence of the solid-state nanoparticles. The distributions of LIs after melting are distinctly different, Figure 4a–c.

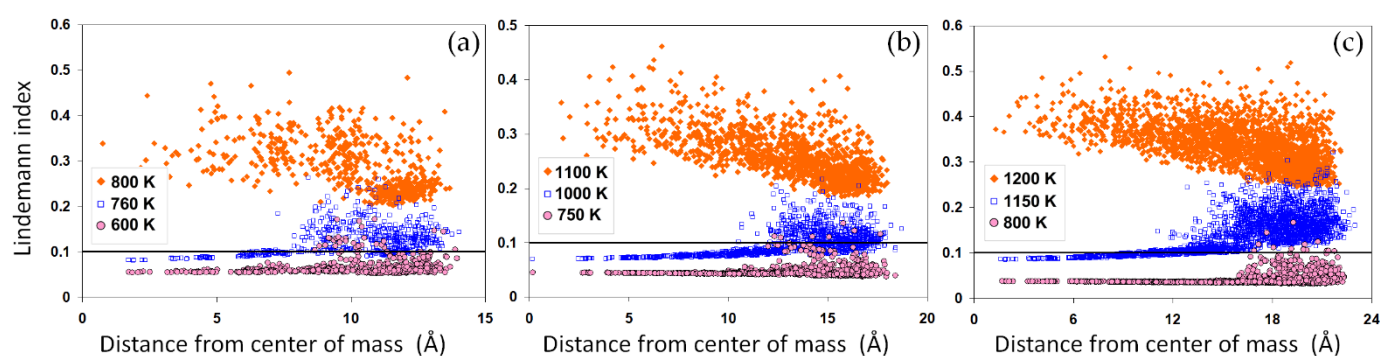


Figure 4. The radial distribution of atomic LI within nanoparticles. The LI distributions are shown for systems with (a) 586, (b) 1289 and (c) 2406 atoms for three temperatures below and at their corresponding melting point. For all systems, a distinct change in the distribution pattern is observed for melted nanoparticles, while a surface premelting (melting below the nominal melting point) is evidenced by the temperature-dependent increase in the LI of the surface atoms. The horizontal line marks the critical LI value 0.1.

The coalescence of the nanoparticles, naturally initiating on their surfaces, is a heterogeneous process and mainly influenced by the energetics and kinetics of the surface atoms. During the coalescence simulations, the initial contact between the two particles is established by the weak attractive forces between them. Figure 5 shows the coalescence of two pairs of Au_{2406} nanoparticles at 1150 and 800 K (initial temperatures). When two nanoparticles touch, a necking region immediately forms. Atomic diffusion takes place, automatically working to reduce the total energy of the system (joined nanoparticles), generally by reducing the high-energy regions. The size evolution of the nanoparticles is exemplified in Figure 5k. The diffusion process and thus the progress in the coalescence strongly depend on the temperature. When the temperature is high enough, e.g., the 1150 K case in Figure 5, the necking rapidly develops towards forming a single larger nanoparticle. The coalescence is much slower at 800 K, developed here up to a necking but preserving the initial outer shape and structure of the nanoparticles. Table 1 lists the minimum full-coalescence temperatures (T_c) measured in our simulations for nanoparticles of different sizes.

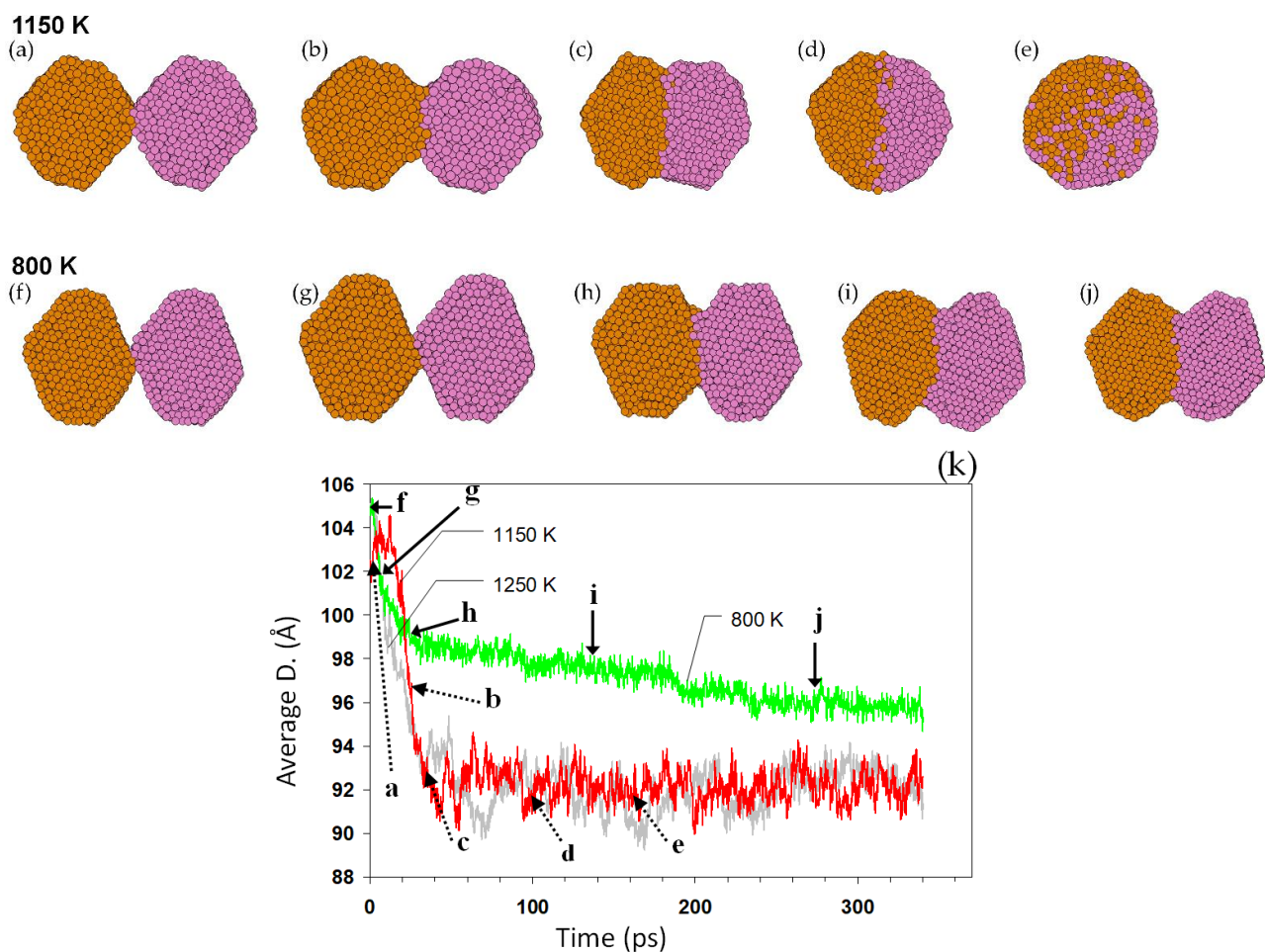


Figure 5. The evolution of coalescing nanoparticles. The snapshots of the coalescence of two pairs of identical 2406 nanoparticles at initial temperatures (a–e) 1150 K and (f–j) 800 K are shown. Cross-sectional views of nanoparticles are shown. The size evolution and the corresponding size/time of the snapshots are shown in (k): a–j in this plot correspond to subfigures (a–j). The size evolution for two liquid nanoparticles at 1250 K is also shown for comparison.

Figure 6a–d show the coalescence of two Au_{2406} nanoparticles at initial temperature 1100 K (solid-state). Figure 6e–g compare the size, potential energy, and the corresponding temperature evolution of this system versus an analogous pairs of nanoparticles coalescing at 1250 K (liquid-state). The size evolution during the two simulations shows a complete coalescence of the nanoparticles for both conditions. Analysis of the potential energy and temperature of the two systems, however, reveals a fundamental difference in the mechanisms of coalescence: For the liquid droplets (at 1250 K), coalescence occurs rapidly with a continuous increase in the temperature, due to the heat released upon the reduction in the total surface area. In the case of the two solid nanoparticles at 1100 K, a nontrivial path is taken in which an initial decrease (increase) in the potential energy (temperature) is inverted during the coalescence, as shown in Figure 6f. This sudden change in the potential energy and temperature indicates a phase transition in the coalescing nanoparticles. The sudden decrease in the energy implies that the energy released due to the surface reduction is invested in *melting* the two coalescing solid nanoparticles (coalescence-induced melting), manifested then by the decrease in the temperature. This reveals synergetic mechanism of coalescence in which the coalescence accelerates itself by the energy released due to the surface reduction, resulting in the melting of solid nanoparticles.

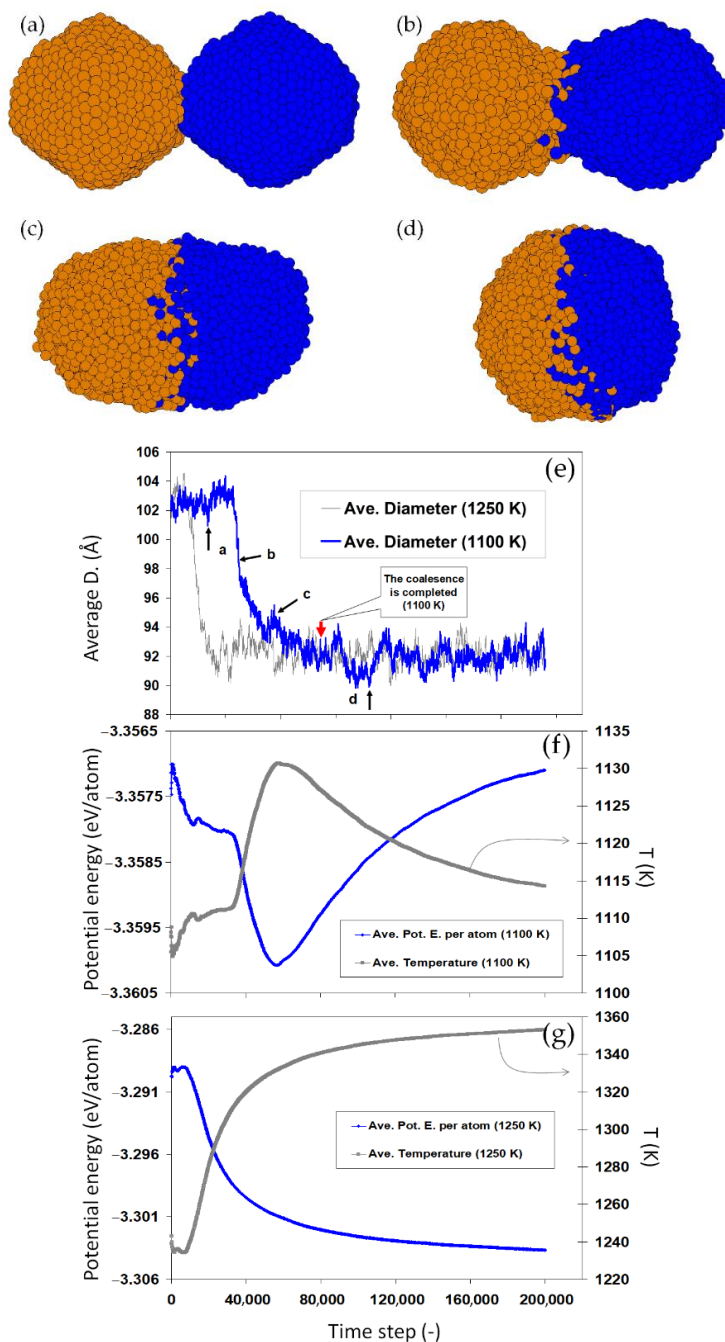


Figure 6. Coalescence of two nanoparticles leading to melting. The shape (a–d), size (e) and energy (f) of two 2406 nanoparticles at 1100 K. A turn in the energy and temperature evolution is observed. The comparison to the coalescence at 1250 K shown in (e,g) reveals a melting transition occurring during the coalescence at 1100 K.

4. Discussion

Coalescence induces size and shape changes in nanoparticles that can have huge impact on their physical properties and functional performance. It is, for instance, demonstrated that the catalytic properties of nanoparticles dramatically change upon coalescence [47]. At elevated temperatures, the nanoparticles' tendency for interaction increases, which is due to the higher atomic mobilities, easing the formation of a larger common interface with surrounding objects. Since almost all properties of nanoparticles are strongly size-dependent, the nanoparticles' coalescence then results in a coupled problem, as it modifies the size distribution as well as the thermal energy distribution within the system.

The current results show that solid-state nanoparticles are able to have a complete coalescence, confirming several previous works [40,43,48]. Our analysis shows that the mechanism of coalescence is surface diffusion (high energy and high mobility surface-atoms). A rapid neck growth and a relatively slow reshaping of the attached nanoparticles were observed, as shown in Figure 5. At higher temperatures, nanoparticles rapidly reshape, while at lower temperatures (for example Au₂₄₀₆ at 800 K, Figure 5) the coalescence begins quickly, but cannot be completed, because of the slow diffusion. Although our simulation times were many orders of magnitude smaller than real experimental times, the coalescence was completed much below their melting points. Thus, in experimental times, it may be expected that even lower coalescence temperatures can be observed given the longer time for diffusion. Because of the surface area reduction, the coalescence is accompanied by an energy release, increasing the temperature, which accelerates the entire process. This confirms previous reports on the sintering process of nanoparticles [49].

Beyond the solid-state coalescence, we found that, in certain conditions, the nominally solid nanoparticles can undergo a melting transition, induced by the energy released upon the coalescence. This is evidenced by a sudden change in the nanoparticles' energy and temperature, as shown in Figure 6. Further simulations of coalescing nanoparticles of different sizes and initial temperatures, as shown in Figure 7, have confirmed this conclusion. The current results establish that the melting transition can be induced for a coalescence of small enough nanoparticles and/or at temperatures close enough to the melting temperature.

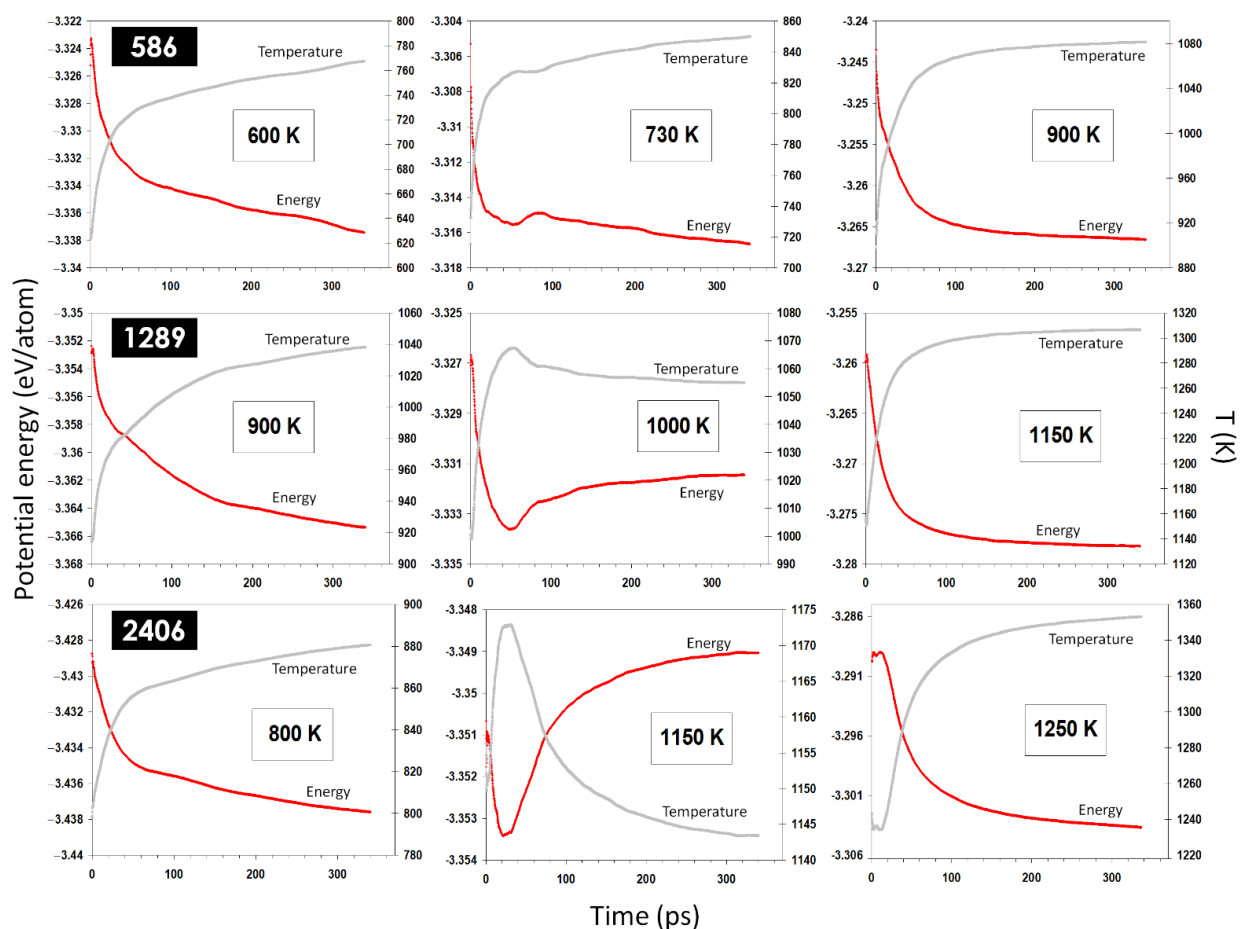


Figure 7. Potential energy and temperature evolution in coalescing nanoparticles of different sizes and at different temperatures. A sudden change in the energy/temperature curves was observed only for temperatures close to the corresponding melting points of the nanoparticles, indicating a surface-induced melting of the nominally solid nanoparticles.

The mechanism of melting during the coalescence can be related to the surface reduction. The energy released due to the surface reduction results in a temperature increase in the system. The simplest approximation of this energy is $\Delta E = \frac{3(2-2^{1/3}) V_m \gamma}{2 r}$ (J/mol), which gives the corresponding increase in the temperature

$$\Delta T = \frac{3(2-2^{1/3}) V_m \gamma}{2 C_p r}. \quad (4)$$

Here, we assume full coalescence, spherical nanoparticles and neglect all additional surface effects and temperature dependence of the properties, with γ the surface energy, V_m the molar volume, C_p the molar heat capacity, and r the radius of the particle. For a gold nanoparticle, considering a surface energy of $\gamma = 1.5 \text{ J/m}^2$, we obtain $\Delta E = \frac{9.48 \times 10^{-6}}{r}$ and $\Delta T = \frac{3.7 \times 10^{-7}}{r}$, that is, for the coalescence of two Au₂₄₀₆ nanoparticles (of a radius about 2.4 nm), we can approximate $\Delta E = 4 \text{ kJ/mol}$ (0.041 eV/atom) and $\Delta T = 154 \text{ K}$. For the melting to occur, the energy released during the coalescence must split between heating up (increasing the temperature) and accommodating the melting latent heat. Thus, the minimum condition for the melting to occur is $\Delta E > L_m$. For the Au₂₄₀₆ system, $L_m = 0.033 \text{ eV/atom}$. As shown Figure 2 and Table 1, the latent heat L_m is also size-dependent, reducing with decreasing the nanoparticle size. This makes the melting even easier during the coalescence of small nanoparticles. Obviously, additional effects, such as stress effects and the effect of surface anisotropy, can play important roles which need further studies.

Besides the surface energy discussed here, more excess energies can be stored in the nanoparticles through lattice defects, which can further contribute to their melting upon coalescence. This mainly depends on the production process. For instance, nanoparticles that are produced in a (nonequilibrium) thermal shock and condensation process are shown to maintain a significant dislocation population and nonequilibrium surface structures [50]. These structural defects carry strain energies which can be released upon the coalescence of nanoparticles. The investigation of these aspects requires the simulation of nonequilibrium nanoparticles, which could be the topic of a future study.

The melting of nanoparticles has been broadly analyzed using differential scanning calorimetry (DSC). Experimental examination of the coalescence-induced melting, however, may need more accurate measurements due to its possible overlap with natural melting upon heating. Simultaneous synchrotron X-ray and DSC analysis can offer a possible route for studying this phenomenon [51]. Two challenges to overcome in such measurements could be the size distribution of nanoparticles being broad and the pre-attachment of nanoparticles before reaching the critical temperature, which, respectively, increases the broadness of the heat curve close to the melting transition and reduces the surface effect. An investigation of a rather narrow size distribution and a good preparation of nanoparticles to remain detached can critically improve the experimental investigation of a coalescence-induced melting phenomenon.

5. Conclusions

We have studied the surface effects on the melting and coalescence of Au nanoparticles of different sizes and at different temperatures, using MD simulations based on the glue potential. The size-dependent melting point and latent heat of nanoparticles were revealed in agreement with previous studies. We analyzed these in terms of the spatial heterogeneous distribution of energy and LI within the nanoparticles. The coalescence of nanoparticles was found to be markedly sensitive to these surface features.

In particular, it has been revealed that the coalescence of two solid nanoparticles may result in the melting of the nanoparticles. This phenomenon is discussed in relation to the surface energy released upon the coalescence, thus making it size- and temperature-dependent. The occurrence of the melting upon coalescence is assisted by the low latent heat

of melting that itself originates in the difference between the solid and liquid nanoparticles' surface energy.

The melting during the coalescence of solid nanoparticles can have important implications for their storage and applications. Our results imply that solid-state nanoparticles applied at intermediate temperature, far below their nominal melting temperature, may still undergo a melting transition upon coalescence. Such a transition then results in a discontinuous change in the physical properties of nanoparticles that can be responsible for a dramatic decline in the performance of nanoparticles. Even single nanoparticles are shown here to have liquid-like surface activities that need to be accounted for during their applications in the intermediate temperature range.

Author Contributions: The current project has been conceptualized, performed, and analyzed by the author. The code for molecular dynamics simulations and the corresponding analytical tools are all developed from scratch. All authors have read and agreed to the published version of the manuscript.

Funding: This research received no external funding.

Data Availability Statement: The data related to this study are available per reasonable request.

Acknowledgments: The current manuscript is in parts a translation from my master thesis on the thermodynamics of nanosystems (in Persian), 2006–2008 [41]. The author would like to thank the discussions with E. Marzban. The author acknowledges the financial supports within the Heisenberg program from DFG, project DA 1655/2-1, which provided the freedom to formulate the research into the current manuscript.

Conflicts of Interest: The authors declare no conflict of interest.

Sample Availability: Samples of the compounds are available from the authors.

References

1. Alivisatos, A.P. Semiconductor Clusters, Nanocrystals, and Quantum Dots. *Science* **1996**, *271*, 933–937. [[CrossRef](#)]
2. Charitidis, C.A.; Georgiou, P.; Koklioti, M.A.; Trompeta, A.-F.; Markakis, V. Manufacturing Nanomaterials: From Research to Industry. *Manuf. Rev.* **2014**, *1*, 11. [[CrossRef](#)]
3. Kruijs, F.E.; Fissan, H.; Peled, A. Synthesis of Nanoparticles in the Gas Phase for Electronic, Optical and Magnetic Applications—A Review. *J. Aerosol Sci.* **1998**, *29*, 511–535. [[CrossRef](#)]
4. Rotello, V. *Nanoparticles: Building Blocks for Nanotechnology*; Springer Science & Business Media: Berlin/Heidelberg, Germany, 2004.
5. He, Z.; Zhang, Z.; Bi, S. Nanoparticles for Organic Electronics Applications. *Mater. Res. Express* **2020**, *7*, 12004. [[CrossRef](#)]
6. Zhang, W.; Zhu, K.; Ren, W.; He, H.; Liang, H.; Zhai, Y.; Li, W. Recent Advances in the Marriage of Catalyst Nanoparticles and Mesoporous Supports. *Adv. Mater. Interfaces* **2022**, *9*, 2101528. [[CrossRef](#)]
7. Yeap, S.P. Permanent Agglomerates in Powdered Nanoparticles: Formation and Future Prospects. *Powder Technol.* **2018**, *323*, 51–59. [[CrossRef](#)]
8. Mandel, K.; Hutter, F. The Magnetic Nanoparticle Separation Problem. *Nano Today* **2012**, *7*, 485–487. [[CrossRef](#)]
9. Minelli, C.; Bartczak, D.; Peters, R.; Rissler, J.; Undas, A.; Sikora, A.; Sjöström, E.; Goenaga-Infante, H.; Shard, A.G. Sticky Measurement Problem: Number Concentration of Agglomerated Nanoparticles. *Langmuir* **2019**, *35*, 4927–4935. [[CrossRef](#)]
10. Contini, C.; Schneemilch, M.; Gaisford, S.; Quirke, N. Nanoparticle–Membrane Interactions. *J. Exp. Nanosci.* **2018**, *13*, 62–81. [[CrossRef](#)]
11. Kurdak, C.; Kim, J.; Farina, L.A.; Lewis, K.M.; Bai, X.; Rowe, M.P.; Matzger, A.J. Au Nanoparticle Clusters: A New System to Model Hopping Conduction. *Turk. J. Phys.* **2004**, *27*, 419–426.
12. Pellegrino, F.; Pellutiè, L.; Sordello, F.; Minero, C.; Ortel, E.; Hodoroaba, V.-D.; Maurino, V. Influence of Agglomeration and Aggregation on the Photocatalytic Activity of TiO₂ Nanoparticles. *Appl. Catal. B Environ.* **2017**, *216*, 80–87. [[CrossRef](#)]
13. Bonaccorso, F.; Zerbetto, M.; Ferrari, A.C.; Amendola, V. Sorting Nanoparticles by Centrifugal Fields in Clean Media. *J. Phys. Chem. C* **2013**, *117*, 13217–13229. [[CrossRef](#)]
14. Qi, W.H.; Wang, M.P. Size and Shape Dependent Melting Temperature of Metallic Nanoparticles. *Mater. Chem. Phys.* **2004**, *88*, 280–284. [[CrossRef](#)]
15. Sardar, R.; Funston, A.M.; Mulvaney, P.; Murray, R.W. Gold Nanoparticles: Past, Present, and Future. *Langmuir* **2009**, *25*, 13840–13851. [[CrossRef](#)]
16. Corma, A.; Garcia, H. Supported Gold Nanoparticles as Catalysts for Organic Reactions. *Chem. Soc. Rev.* **2008**, *37*, 2096–2126. [[CrossRef](#)] [[PubMed](#)]
17. Tran, T.D.; Nguyen, M.T.T.; Le, H.V.; Nguyen, D.N.; Truong, Q.D.; Tran, P.D. Gold Nanoparticles as an Outstanding Catalyst for the Hydrogen Evolution Reaction. *Chem. Commun.* **2018**, *54*, 3363–3366. [[CrossRef](#)] [[PubMed](#)]

18. Thompson, D.T. Using Gold Nanoparticles for Catalysis. *Nano Today* **2007**, *2*, 40–43. [[CrossRef](#)]
19. Bacalzo, N.P., Jr.; Go, L.P.; Querebillo, C.J.; Hildebrandt, P.; Limpoco, F.T.; Enriquez, E.P. Controlled Microwave-Hydrolyzed Starch as a Stabilizer for Green Formulation of Aqueous Gold Nanoparticle Ink for Flexible Printed Electronics. *ACS Appl. Nano Mater.* **2018**, *1*, 1247–1256. [[CrossRef](#)]
20. Daniel, M.-C.; Astruc, D. Gold Nanoparticles: Assembly, Supramolecular Chemistry, Quantum-Size-Related Properties, and Applications toward Biology, Catalysis, and Nanotechnology. *Chem. Rev.* **2004**, *104*, 293–346. [[CrossRef](#)]
21. Guzzi, L.; Horváth, D.; Pászti, Z.; Tóth, L.; Horváth, Z.E.; Karacs, A.; Peto, G. Modeling Gold Nanoparticles: Morphology, Electron Structure, and Catalytic Activity in CO Oxidation. *J. Phys. Chem. B* **2000**, *104*, 3183–3193. [[CrossRef](#)]
22. Li, D.; He, Q.; Li, J. Smart Core/Shell Nanocomposites: Intelligent Polymers Modified Gold Nanoparticles. *Adv. Colloid Interface Sci.* **2009**, *149*, 28–38. [[CrossRef](#)] [[PubMed](#)]
23. Shibata, N.; Goto, A.; Matsunaga, K.; Mizoguchi, T.; Findlay, S.D.; Yamamoto, T.; Ikuhara, Y. Interface Structures of Gold Nanoparticles on TiO₂ (110). *Phys. Rev. Lett.* **2009**, *102*, 136105. [[CrossRef](#)]
24. Haruta, M.; Daté, M. Advances in the Catalysis of Au Nanoparticles. *Appl. Catal. A Gen.* **2001**, *222*, 427–437. [[CrossRef](#)]
25. Magnusson, M.H.; Deppert, K.; Malm, J.-O.; Bovin, J.-O.; Samuelson, L. Gold Nanoparticles: Production, Reshaping, and Thermal Charging. *J. Nanopart. Res.* **1999**, *1*, 243–251. [[CrossRef](#)]
26. Qi, W.H. Size Effect on Melting Temperature of Nanosolids. *Phys. B Condens. Matter* **2005**, *368*, 46–50. [[CrossRef](#)]
27. Ercolessi, F.; Parrinello, M.; Tosatti, E. Simulation of Gold in the Glue Model. *Philos. Mag. A* **1988**, *58*, 213–226. [[CrossRef](#)]
28. Ercolessi, F.; Adams, J.B. Interatomic Potentials from First-Principles Calculations: The Force-Matching Method. *EPL Europhys. Lett.* **1994**, *26*, 583. [[CrossRef](#)]
29. Ercolessi, F.; Adams, J.B. Interatomic Potentials from First-Principles Calculations. *MRS Online Proc. Libr.* **1992**, *291*, 31. [[CrossRef](#)]
30. Pan, H.; Ko, S.H.; Grigoropoulos, C.P. The Solid-State Neck Growth Mechanisms in Low Energy Laser Sintering of Gold Nanoparticles: A Molecular Dynamics Simulation Study. *J. Heat Transf.* **2008**, *130*, 092404. [[CrossRef](#)]
31. Fedorov, A.V.; Shulgin, A.V. Complex Modeling of Melting of an Aluminum Nanoparticle. *Combust. Explos. Shock Waves* **2013**, *49*, 442–449. [[CrossRef](#)]
32. Shi, Z.; Wynblatt, P.; Srinivasan, S.G. Melting Behavior of Nanosized Lead Particles Embedded in an Aluminum Matrix. *Acta Mater.* **2004**, *52*, 2305–2316. [[CrossRef](#)]
33. Chui, Y. *Molecular Dynamics Study of Structure and Stability in Au Nanoparticles*; RMIT University: Melbourne, Australia, 2007.
34. Bussi, G.; Donadio, D.; Parrinello, M. Canonical Sampling through Velocity Rescaling. *J. Chem. Phys.* **2007**, *126*, 14101. [[CrossRef](#)] [[PubMed](#)]
35. Allen, M.P.; Tildesley, D.J. *Computer Simulation of Liquids*; Oxford University Press: Oxford, UK, 2017.
36. Barmparis, G.D.; Lodziana, Z.; Lopez, N.; Remediakis, I.N. Nanoparticle Shapes by Using Wulff Constructions and First-Principles Calculations. *Beilstein J. Nanotechnol.* **2015**, *6*, 361–368. [[CrossRef](#)] [[PubMed](#)]
37. Lindemann, F.A. Physics of the Lindemann Melting Rule. *Phys. Z* **1910**, *11*, 609.
38. Proykova, A.; PISOV, S.; Radev, R.; Mihailov, P.; Daykov, I.; Berry, R.S. Temperature Induced Phase Transformations of Molecular Nanoclusters. *Vacuum* **2002**, *68*, 87–95. [[CrossRef](#)]
39. Jiang, A.; Awasthi, N.; Kolmogorov, A.N.; Setyawan, W.; Börjesson, A.; Bolton, K.; Harutyunyan, A.R.; Curtarolo, S. Theoretical Study of the Thermal Behavior of Free and Alumina-Supported Fe-C Nanoparticles. *Phys. Rev. B* **2007**, *75*, 205426. [[CrossRef](#)]
40. Ding, F.; Rosén, A.; Bolton, K. Size Dependence of the Coalescence and Melting of Iron Clusters: A Molecular-Dynamics Study. *Phys. Rev. B* **2004**, *70*, 75416. [[CrossRef](#)]
41. Kamachali, R.D. *Investigation on the Extensivity and Intensivity of Thermodynamic Parameters of Nanosystems Using Molecular Dynamic Simulation Method*; Materials & Energy Research Centre: Karaj, Iran, 2008.
42. Di Tolla, F.D.; Ercolessi, F.; Tosatti, E. Maximum Overheating and Partial Wetting of Nonmelting Solid Surfaces. *Phys. Rev. Lett.* **1995**, *74*, 3201. [[CrossRef](#)]
43. Arcidiacono, S.; Bieri, N.R.; Poulikakos, D.; Grigoropoulos, C.P. On the Coalescence of Gold Nanoparticles. *Int. J. Multiph. Flow* **2004**, *30*, 979–994. [[CrossRef](#)]
44. Buffat, P.; Borel, J.P. Size Effect on the Melting Temperature of Gold Particles. *Phys. Rev. A* **1976**, *13*, 2287. [[CrossRef](#)]
45. Jiang, H.; Moon, K.; Dong, H.; Hua, F.; Wong, C.P. Size-Dependent Melting Properties of Tin Nanoparticles. *Chem. Phys. Lett.* **2006**, *429*, 492–496. [[CrossRef](#)]
46. Xiong, S.; Qi, W.; Cheng, Y.; Huang, B.; Wang, M.; Li, Y. Universal Relation for Size Dependent Thermodynamic Properties of Metallic Nanoparticles. *Phys. Chem. Chem. Phys.* **2011**, *13*, 10652–10660. [[CrossRef](#)] [[PubMed](#)]
47. Li, T.; Wang, J.; Wang, F.; Zhang, L.; Jiang, Y.; Arandiyán, H.; Li, H. The Effect of Surface Wettability and Coalescence Dynamics in Catalytic Performance and Catalyst Preparation: A Review. *ChemCatChem* **2019**, *11*, 1576–1586. [[CrossRef](#)]
48. Grammatikopoulos, P.; Sowwan, M.; Kioseoglou, J. Computational Modeling of Nanoparticle Coalescence. *Adv. Theory Simul.* **2019**, *2*, 1900013. [[CrossRef](#)]
49. Lehtinen, K.E.J.; Zachariah, M.R. Effect of Coalescence Energy Release on the Temporal Shape Evolution of Nanoparticles. *Phys. Rev. B* **2001**, *63*, 205402. [[CrossRef](#)]

-
50. Liu, S.; Hu, Z.; Wu, Y.; Zhang, J.; Zhang, Y.; Cui, B.; Liu, C.; Hu, S.; Zhao, N.; Han, X. Dislocation-Strained IrNi Alloy Nanoparticles Driven by Thermal Shock for the Hydrogen Evolution Reaction. *Adv. Mater.* **2020**, *32*, 2006034. [[CrossRef](#)]
 51. Higami, M.; Ueno, S.; Segawa, T.; Iwanami, K.; Sato, K. Simultaneous Synchrotron Radiation X-Ray Diffraction-DSC Analysis of Melting and Crystallization Behavior of Trilauroylglycerol in Nanoparticles of Oil-in-Water Emulsion. *J. Am. Oil Chem. Soc.* **2003**, *80*, 731–739. [[CrossRef](#)]